CHAPTER 4

Synthesis of graphene oxide-polyaniline-copper cobaltite ($GO/PANI/CuCo_2O_4$) based hybrid composite system and its use in supercapacitor electrodes

4.1. Introduction

The main goal of the current research is to improve the cycle life while also increasing the system's specific capacitance, coulombic efficiency, specific energy, and specific power. In review literature (chapter 2), it has been observed that composite systems exhibit superior electrochemical performances than the individual materials. However, sometimes composites also exhibit inferior electrochemical activity than the individual constituents mainly due to under explored active sites and pore blockage of the systems [189,206]. In this chapter, a comparison in the electrochemical properties of graphene oxide-polyaniline-copper cobaltite based ternary composite with the single and binary systems has been done. All the calcined metal oxides (MOx) were taken into consideration. Graphene oxide was successfully synthesized using the modified Hummers method by taking natural graphite flake powder as a raw material. For this study, the weight ratio of both, GO:aniline and aniline:$CuCo_2O_4$ (copper cobaltite) were taken as 1:4 and 4:1, respectively. The weight ratio of GO:aniline:$CuCo_2O_4$ was fixed at 1:4:1. Since, polyaniline is a conducting polymer, it provides excellent conducting networks inside a composite system. Similarly, metal oxides support multiple redox transitions and helps in increasing the energy density. However, carbon based materials provide better structural stability in the system and enhance the power density as well, but they have less contribution to the energy density. So, polyaniline was used at a higher amount to maintain a stable electrical connection within the system and get a good energy density. Excessive use of metal oxides can block the active pores and reduce the electrochemical performance. So, the ratio of 1:4:1 has been chosen for ternary composite based electrodes. All the experimental details have been given in section 3.2.1 to 3.2.5.

4.2. Results and discussion

4.2.1. Raman Spectra

To confirm the formation of GO, Raman spectroscopy was performed. In figure 4.1, D-band was observed at 1346.09 cm^{-1} while the G-band at 1598.20 cm^{-1}. Disorder factors are considered based on defects, i.e., grain, vacancies, boundaries, and amorphous carbon species. The band intensity ratio, I_D/I_G was measured with the value of 1.04 for GO, which showed the interstitial repair in aromatic structures. The peak at low intensity (2696.22 cm^{-1}) represents graphene oxide layers with fewer defects and is attributed to the low oxygen content in graphene oxide. In addition, the peak at 2921.53 cm^{-1} (2D-band) shows a reduction in defects. Overall, increased peak intensities show the degree of graphitization.

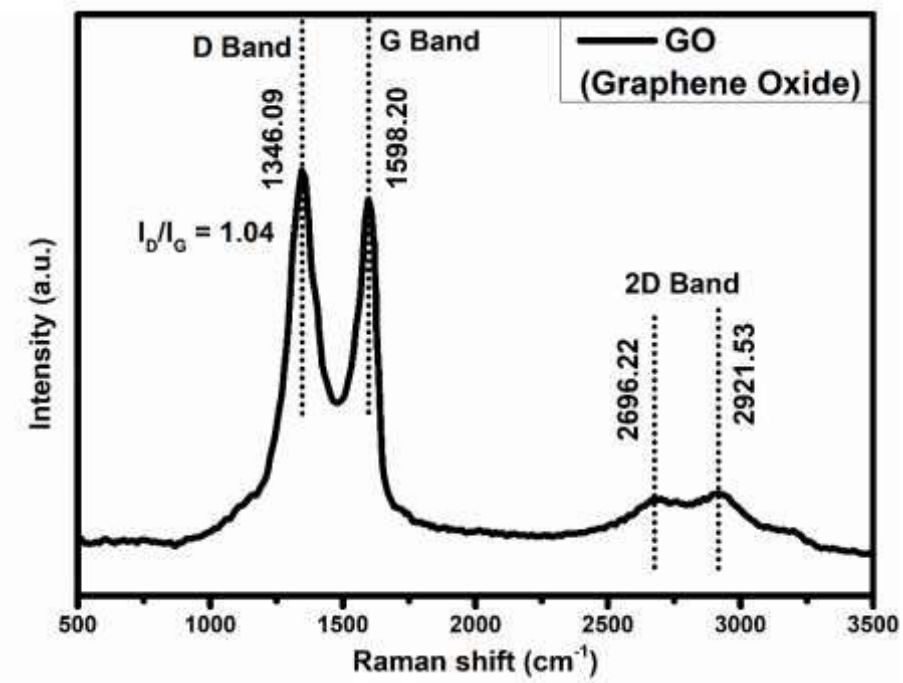

Figure 4.1: Raman spectra of GO

4.2.2. XRD analysis

The XRD patterns of GO, GO/PANI, PANI/$CuCo_2O_4$, and GO/PANI/$CuCo_2O_4$ have been done in the range of 10°-80°, the results are given in figure 4.2 (a). The characteristics peak of GO is positioned at 2θ = 11.05° (001) and the existence of a small peak at 2θ = 42.29° (100) is due to the presence of the small amount of graphite phases [185]. Peaks at 2θ = 20.16° (020) and 25.21° (200) confirmed the synthesis of pure polyaniline. 2θ intense peaks at 20.37° (020), 25.24° (200) and a small peak at 42.55° (100) give the confirmation of GO/PANI composite. The diffraction peaks for pure $CuCo_2O_4$ has been seen at 19.08° (111), 31.33° (220), 35.62° (444), 36.84° (311), 38.86° (222), 44.91° (400), 59.44° (511), and 65.23° (440) [JCPDS 01-1155] [207]. In the case of PANI/$CuCo_2O_4$, peaks at 20.37° (020), 25.24° (200), 31.19° (220), 36.79° (311), 44.82° (400), 59.30° (511), and 65.25° (440) evidence the formation of PANI/$CuCo_2O_4$ composite. The ternary composite of GO/PANI/$CuCo_2O_4$ consists peaks at 20.56° (020), 25.25° (200), 31.90° (220), 36.79° (311), 42.72° (110), 44.65° (400), 59.30° (511) and 65.06° (440) as shown in table 4.1. The slight shifting of the characteristic peaks is mainly due to the increase and decrease of the crystallite sizes of the GO, PANI, and $CuCo_2O_4$. The intense peak of GO at 11.05° (001) could not be seen in the GO/PANI and GO/PANI/$CuCo_2O_4$ composite due to the interaction between the individual materials and folding of the disordered chain of polyaniline.

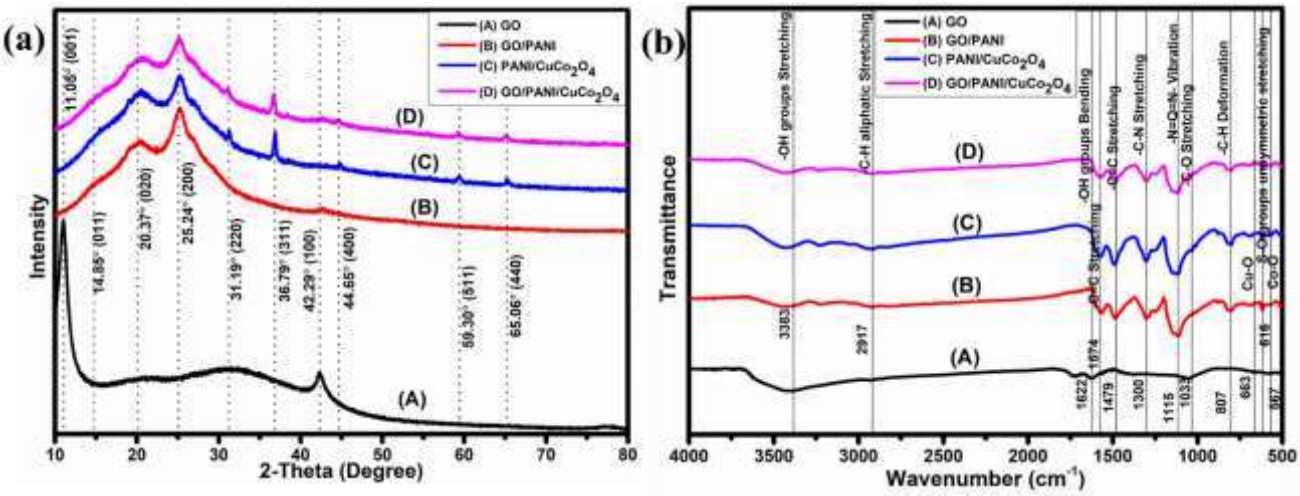

Figure 4.2: (a) XRD pattern. (b) FTIR spectrum of prepared samples

Table 4.1: Peak and hkl values of GO/PANI/$CuCo_2O_4$

Peaks	Diffraction angle (in degree)	hkl
1	14.85	011
2	20.37	020
3	25.24	200
4	31.19	220
5	36.79	311
6	42.29	100
7	44.65	400
8	59.30	511
9	65.06	440

From the XRD analysis, interlayer spacing (d) evaluated by using Bragg's law (equation 4.1) and the crystallite size (L) can be determined by the help of Scherrer equation (equation 3.4) [208].

$$d = \frac{\lambda}{2.\sin\theta} \text{ (Bragg's law)} \quad (4.1)$$

- λ, radiation wavelength (λ = 0.154 nm)
- θ, diffraction peak position in degree

Table 4.2: Characteristics of different samples via XRD method

Sample	FWHM (°)	d(nm)	L(nm)
GO	0.87	0.80	9.58
GO/PANI	1.02	0.35	8.34
PANI/$CuCo_2O_4$	0.33	0.24	25.74
GO/PANI/$CuCo_2O_4$	0.39	0.24	22.31

The characteristic parameters like interlayer spacing and crystallite size of different samples are listed in table 4.2. The decrease in the interlayer spacing compared to GO mainly occurs due to the deformation of the polyaniline chain and the reduction of different intercalated oxygen functional groups which form the conjugated system of π-bond on GO sheets [56]. It was calculated that crystallite size decrease from 9.58 nm in GO to 8.34 nm in GO/PANI and further increases to 25.74 nm in PANI/$CuCo_2O_4$, 22.31 nm in GO/PANI/$CuCo_2O_4$ which is basically dependent upon the degree of oxidation and reduction [208].

4.2.3. FTIR Analysis

The FTIR spectrum of GO, GO/PANI, PANI/$CuCo_2O_4$, and GO /PANI/$CuCo_2O_4$ have been displayed in figure 4.2 (b) to identify the different types of functional groups. For GO, the spectrum at 3383 cm^{-1} is because of O-H groups stretching vibration. Similarly, bands at 2917 cm^{-1} and 1622 cm^{-1} correspond to aliphatic C-H stretching and bending of O-H groups. A peak at around 1033 cm^{-1} is due to the stretching vibration of -C-O [209]. The characteristic peak at 1622 cm^{-1} is related to O-H groups bending of GO, which is also existing in GO/PANI and GO/PANI/$CuCo_2O_4$. In the case of polyaniline, the band at 807 cm^{-1} signifies the C-H deformation and the spectrum at 1115 cm^{-1} is due to the N=Q=N stretching vibration. moreover, the band at 1300 cm^{-1} corresponds to the C-N stretching vibration in the quinoid ring, which is the indication of conducting polyaniline behavior. Spectroscopic peaks at 1479 cm^{-1} and 1574 cm^{-1} indicate the C=C stretching vibration based on benzene and quinone rings, respectively [29,210]. The band at 616 cm^{-1} could be because of the unsymmetrical stretching of S-O groups in PTSA-PANI. For $CuCo_2O_4$, peaks at 567 cm^{-1} for Co-O and 663 cm^{-1} due to Cu-O [211,212]. Compared to GO in figure 4.2 (b), the band at 3383 cm^{-1} in the curve (B) and (D) becomes smooth and wide, which is due to the consumption of carboxyl and hydroxyl groups on the GO/PANI and GO/PANI/$CuCo_2O_4$ surface during the time of reaction, which resulted in the decrease in band intensity. The slightest variation of spectroscopic PANI bands in GO/PANI, PANI/$CuCo_2O_4$ and GO/PANI/$CuCo_2O_4$ could be because of its interrelation and chemical interaction with GO and $CuCo_2O_4$, resulting in increased delocalized charges in the backbone of PANI.

4.2.4. FESEM

Surface diagnosis of the different samples was inspected by the FE-SEM and shown in figure 4.3. The image of graphene oxide in figure 4.3 (a) resembles that graphene oxide has a sheet-

like structure and multiple stacks exist with very thin sheets. On the other side, polyaniline seems like an agglomeration of rod-like structure, whereas $CuCo_2O_4$ is a polyhedral shape structure with some irregularities. In GO/PANI, the polyaniline particles may have dispersed and uniformly distributed onto the graphene oxide layers, so that is why only rod-like particles are seen in the image. In PANI/$CuCo_2O_4$, the $CuCo_2O_4$ particles may have dispersed into the polyaniline rod-like structure. Due to this, the polyhedral texture of $CuCo_2O_4$ does not look in the PANI/$CuCo_2O_4$, and only rod-like shapes with an agglomeration of PANI particles are noticed. The structure of GO/PANI/$CuCo_2O_4$ is similar to PANI/$CuCo_2O_4$ because of the uniform distribution of rod-like particles over layered graphene oxide and the dispersion of $CuCo_2O_4$ particles into PANI. The addition of sonicated GO and $CuCo_2O_4$ might have changed the micelle structure, which formed during dropwise addition of aniline in PTSA solution, and this changed into rod-like textures when dropwise addition of APS starts [213].

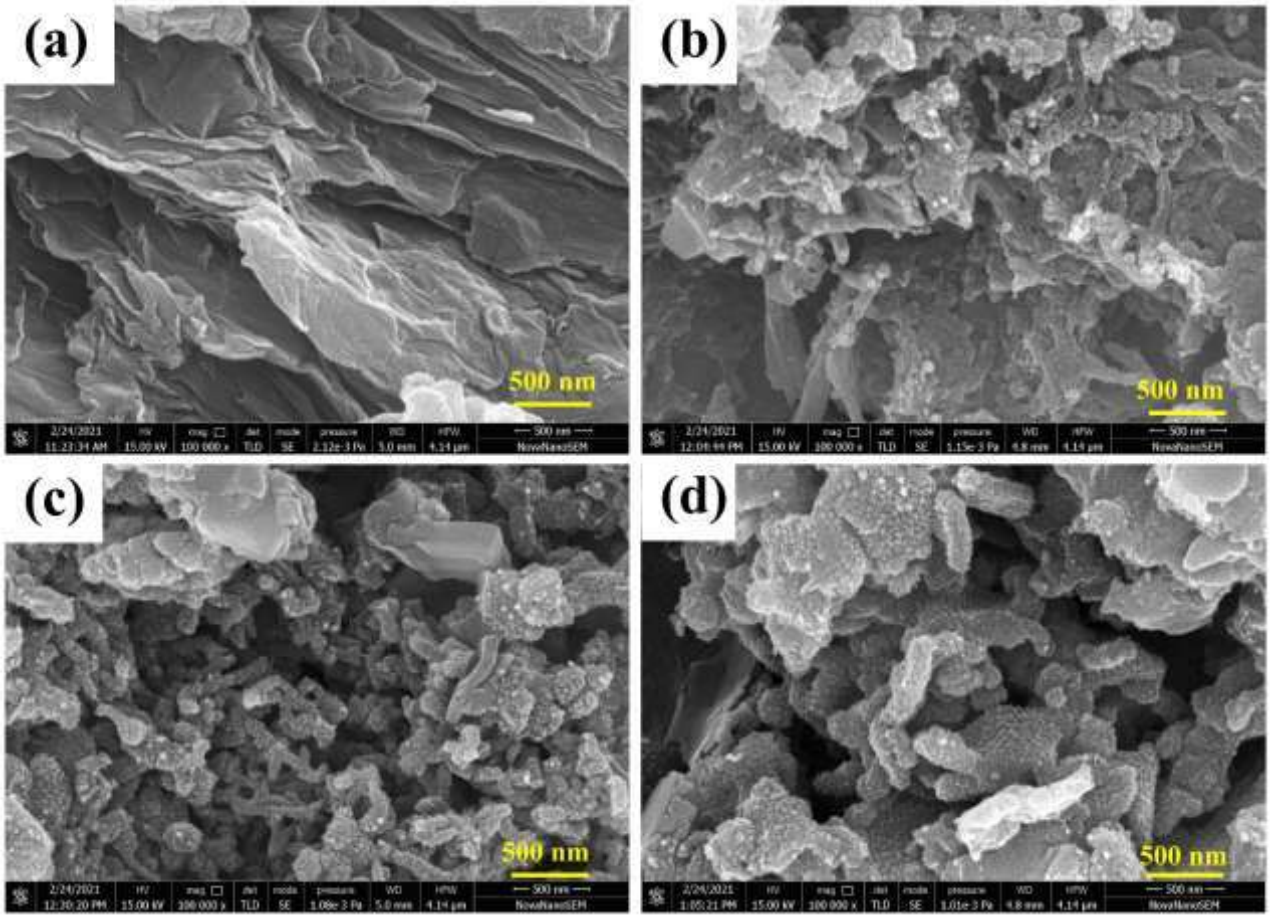

Figure 4.3: FE-SEM images of (a) GO. (b) GO/PANI. (c) PANI/$CuCo_2O_4$. (d) GO/PANI/$CuCo_2O_4$

4.2.5. Compositional analysis from surface morphology

The complete detailed data about the atomic% and weight% of every single atom in the composites has been shown in figure 4.4. The attached tables and the spectrum clearly illustrated that the proportion of Cu:Co is nearly equal to the atomic composition which was used at the time of composite synthesis. The presence of sulfur in case of graphene oxide is due to the addition of sulfuric acid during the synthesis process. In case of composites of graphene oxide, the existence of sulfur and nitrogen are due to the addition of PTSA and APS, respectively [207].

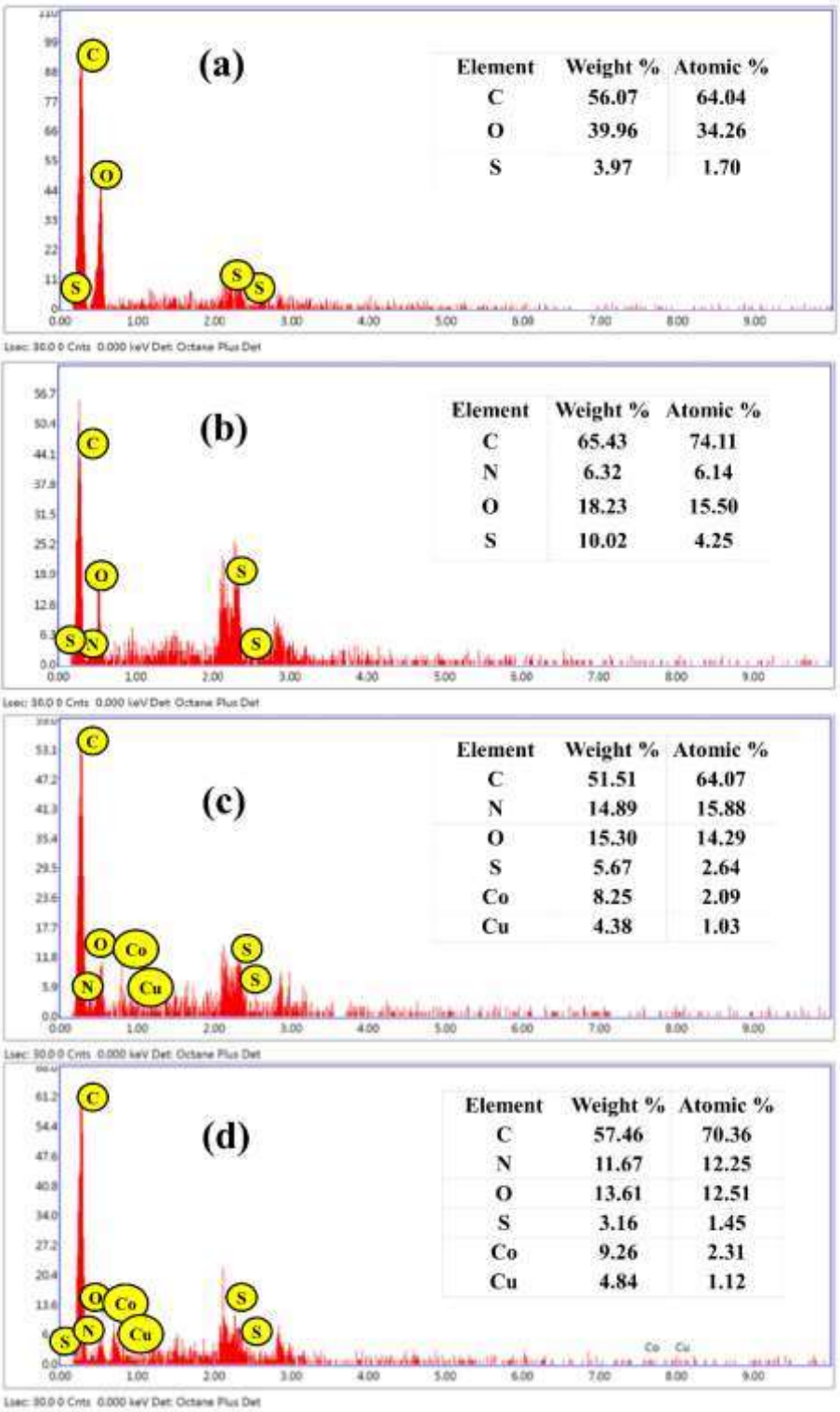

Figure 4.4: EDS of (a) GO. (b) GO/PANI. (c) PANI/$CuCo_2O_4$. (d) GO/PANI/$CuCo_2O_4$

Elemental mapping of all prepared materials has been shown in figure 4.5. From the mapping, it could be seen that the components are uniformly distributed in the composite. This proves the successful synthesis of ternary composite and integrity of the components.

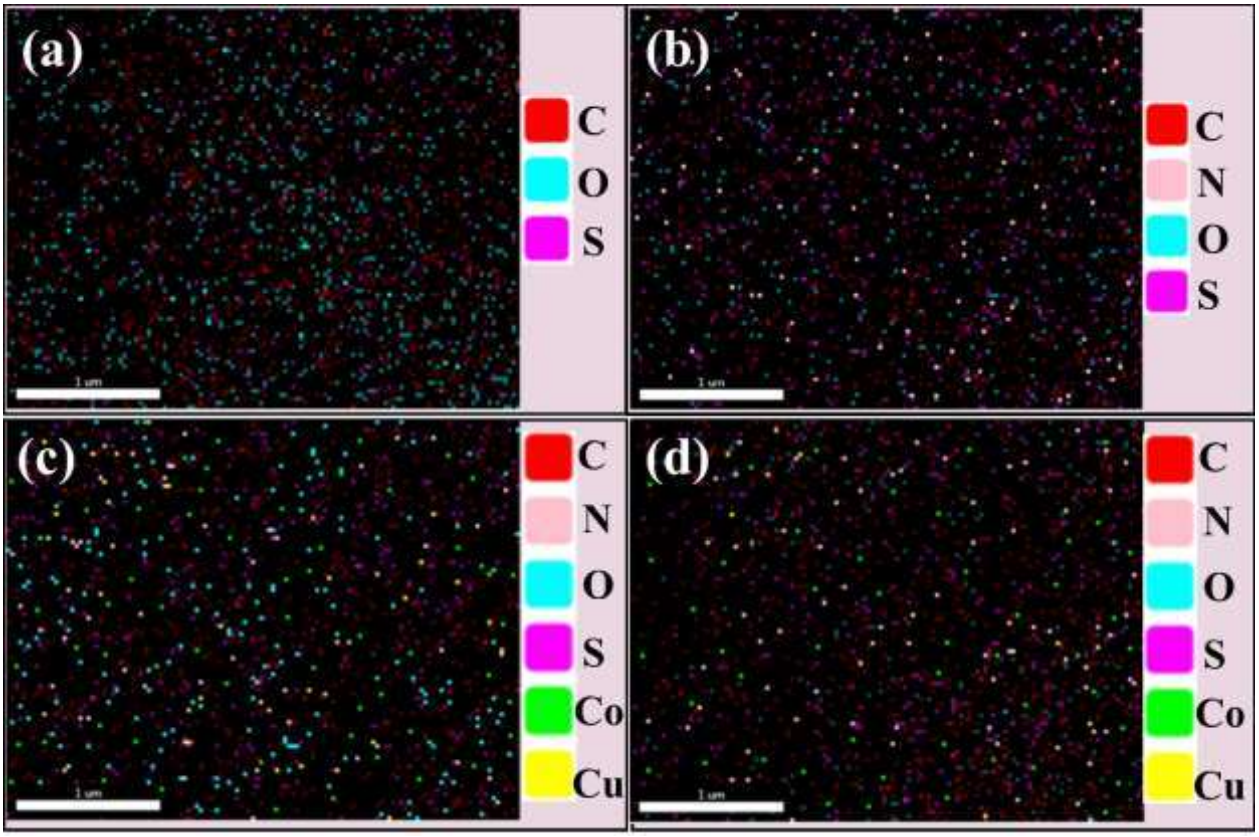

Figure 4.5: Elemental mapping of (a) GO. (b) GO/PANI. (c) PANI/$CuCo_2O_4$. (d) GO/PANI/$CuCo_2O_4$

4.2.6. Electrochemical characterization

The electrochemical performance of the prepared electrodes has been noticed by the CV and CD. The CV plot of all the prepared electrodes in a three-electrode configuration system at a constant 1 mV/s scan rate is given in figure 4.6 (a). CV nature of ternary composite GO/PANI/$CuCo_2O_4$ also has been explored at different scan rates of 1, 2, 5, 10, and 20 mV/s and given in figure 4.6 (b).

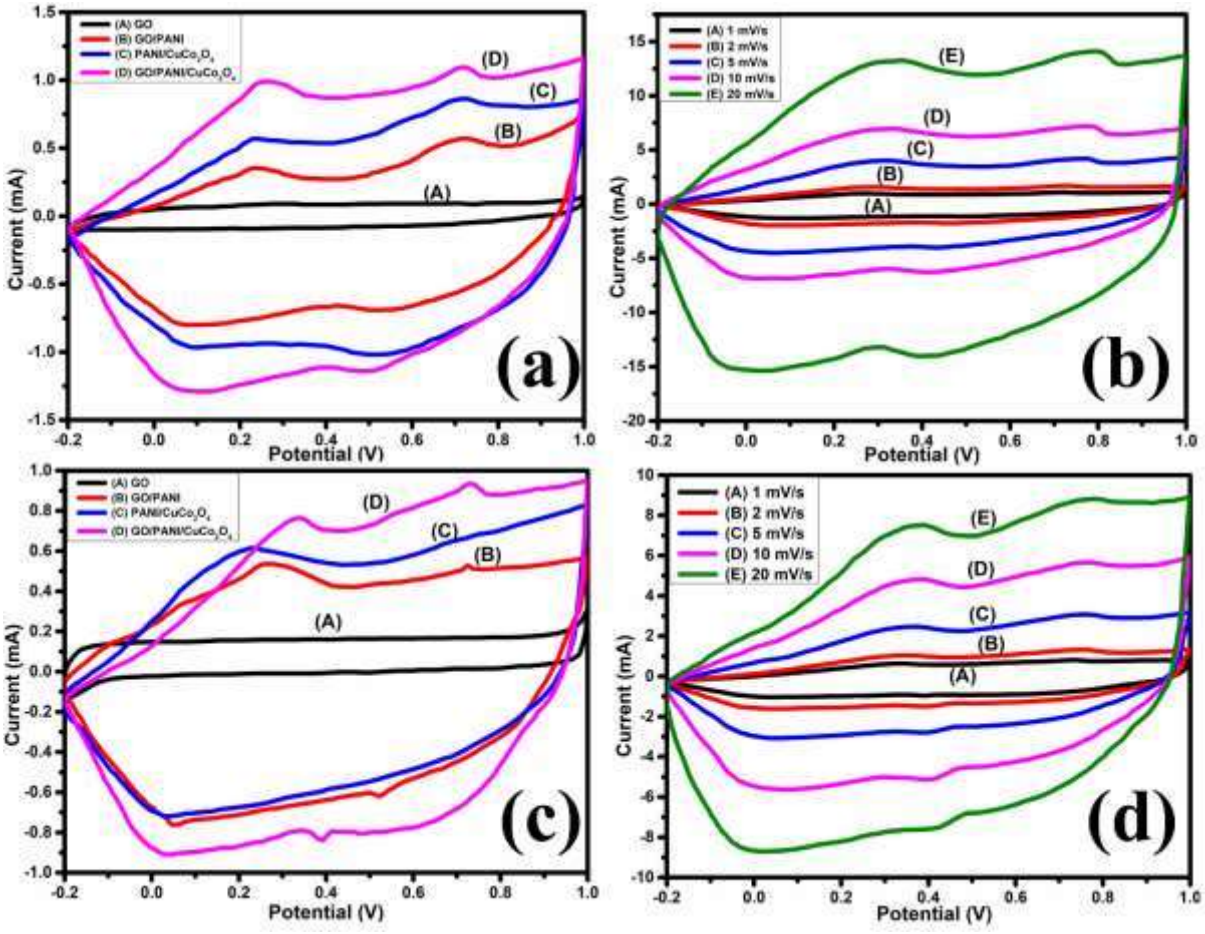

Figure 4.6: CV curve of different samples at (a) 1 mV/s using three-electrode system. (b) Different scan rates using three-electrode system. (c) 1 mV/s using symmetric two-electrode system. (d) Different scan rates using symmetric two-electrode system

In figure 4.6 (a) nearly rectangular-shaped CV plot (A) is for GO, which is carbon-based material and shows the EDLC nature of the system. Generally, there are three reduction-oxidation peaks of pristine PANI positioned at 0.13 V, 0.42 V, 0.62 V denoting the reduction states and 0.28 V, 0.58 V, 0.71 V corresponding to the oxidation states. The oxidation peak at 0.28 V is due to the conversion of leucoemeraldine salt to emeraldine salt and at 0.58 V is

allocated to the degradation state of hydroquinone/benzoquinone. Conversion of emeraldine to pernigraniline is attributed to 0.71 V [87]. Figure 4.7 displays the various transition states of PANI [199].

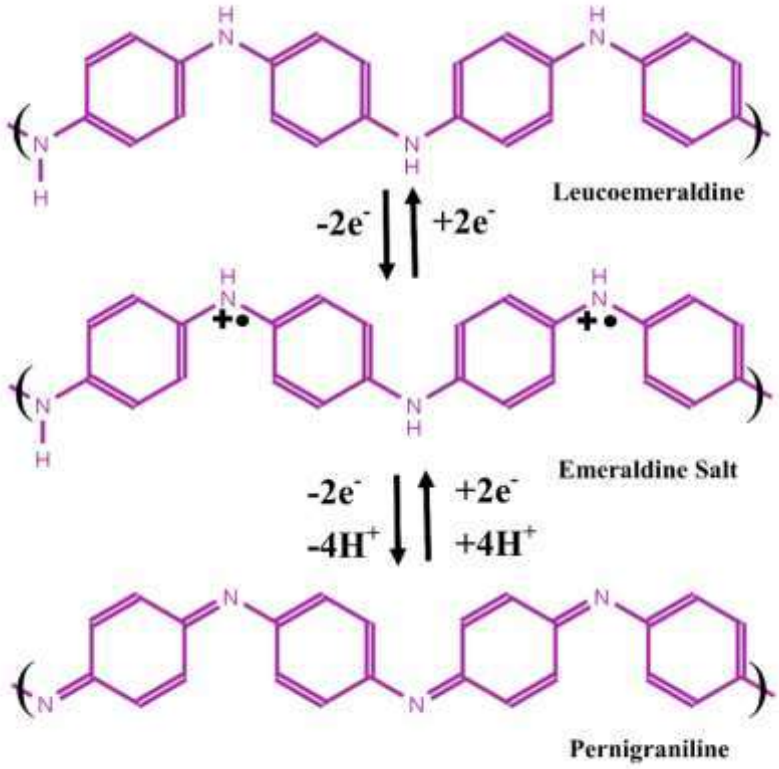

Figure 4.7: Different transition states of polyaniline

The binary composite of GO/PANI indicated redox (oxidation-reduction) peaks and represent the pseudocapacitance behavior due to the existence of PANI. The CV plot of binary GO/PANI conveys the combined nature of EDLC and pseudocapacitance. From figure 4.6 (a), it can be seen that the voltammetric area of GO/PANI is larger than the voltammetric area of GO, which means more specific capacitance of binary GO/PANI than pristine GO. The oxidation peaks at 0.3 V and 0.4 V are corresponding to the Co^{3+}/Co^{4+} and

Cu^{2+}/Cu^{3+} transition in $CuCo_2O_4$ [214]. $CuCo_2O_4$ goes through the following electrochemical reactions (equation 4.2 to 4.4) [212].

$$CuCo_2O_4 + H_2O + OH^- \leftrightarrow 2CoOOH + CuOOH + e^- \quad (4.2)$$

$$CoOOH + OH^- \leftrightarrow CoO_2 + H_2O + e^- \quad (4.3)$$

$$CuOH + OH^- \leftrightarrow Cu(OH)_2 + e^- \quad (4.4)$$

For the binary GO/PANI, PANI/$CuCo_2O_4$, and ternary GO/PANI/$CuCo_2O_4$, the oxidation peak at around 0.58 V disappeared, which could be mainly due to the involvement of GO and $CuCo_2O_4$ particles [207]. The oxidation peaks of $CuCo_2O_4$ are not seen in binary PANI/$CuCo_2O_4$ and ternary GO/PANI/$CuCo_2O_4$ because metal oxides (i.e. $CuCo_2O_4$) have high density and graphene oxide possesses high surface area. The metal oxide may be dispersed into the graphene oxide pores and the surface of metal oxide and graphene oxide may be covered with PANI structure. PANI shows conducting nature and could be easily seen from the FE-SEM image (figure 4.5) of binary PANI/$CuCo_2O_4$ and ternary GO/PANI/$CuCo_2O_4$ that mainly rod-type structure is seen. So, when the electrochemical reactions happen on the composite surface, the oxidation-reduction peaks of PANI are mainly observed and not the peaks of $CuCo_2O_4$. The incorporation of GO and $CuCo_2O_4$ could intensify the activity of binary and ternary composite, and avoid the synthesis of devalued products [211]. Figure 4.6 (a) represents the high value of peak current and specific capacitance for GO/PANI/$CuCo_2O_4$ due to well-interconnected patterns and high voltammetric area than binary GO/PANI, PANI/$CuCo_2O_4$, and GO. This uniform interconnecting rod-like pattern and porous GO structure of ternary GO/PANI/$CuCo_2O_4$ is responsible for better movement of ions and gives a high peak current. The CV plot for

GO/PANI/$CuCo_2O_4$ composite at different scan rates is displayed in figure 4.6 (b). The voltammetric area as well as peak current increases with increasing the scan rate. Here the acquired current is the combined effect of capacitive and faradaic current. As the scan rate is increased, the contact time of electrolyte ions and electroactive species at the active sites is very less, so specific capacitance decreases with increasing the scan rates. The energy stored in a supercapacitor is due to combined nature of pseudocapacitance and EDLC, but with increasing scan rate, the contribution of pseudocapacitance decreases. Equation 4.5 was applied to evaluate the specific capacitance value (C_s) from the CV three-electrode system;

$$C_s = \frac{\int IdV}{ma * \nu * \Delta V} \text{ [Three-electrode CV]} \quad (4.5)$$

C_s = Specific capacitance of the working electrode obtained from three-electrode CV curve (F/g); $\int IdV$ = cathodic scan CV area; ma = active material mass (mg); ν = scan rate (mV/s); ΔV = stable potential window (Volt)

The behavior of the formed electrodes has also been evaluated by using a symmetric two-electrode (2E) symmetric system. Equations 4.6 and 4.7 are applied to compute the specific capacitance value from symmetric two-electrode CV and CD, respectively.

$$C_s = \frac{\int IdV}{mt * \nu * \Delta V} \text{ [Two-electrode CV]} \quad (4.6)$$

$$C_s = \frac{I * td}{mt * \Delta V} \text{ [Two-electrode CD]} \quad (4.7)$$

C_s = specific capacitance obtained from two-electrode (2E) system (F/g); $\int IdV$ = cathodic CV area; I = discharge current (mA); t_d = discharge time (s); mt = total active mass (mg); ν = scan rate (mV/s); ΔV = stable potential window (Volt)

From the symmetric two-electrode CV plot, it could be seen that GO/PANI/$CuCo_2O_4$ ternary composite has a higher peak current value than other fabricated electrodes at 1 mV/s scan rate (figure 4.6 (c)). The combined behavior of EDLC (GO) and pseudocapacitive (PANI, $CuCo_2O_4$) material results in various redox reactions. High electron mobility in the ternary composite GO/PANI/$CuCo_2O_4$ is responsible for high peak current and high voltammetric area than others. Hence, the specific capacitance of ternary composite is the highest among all the prepared electrodes. Figure 4.6 (d) gives the details about the effect of the voltammetric area with increasing scan rate for ternary composite GO/PANI/$CuCo_2O_4$. It can be concluded that the value of maximum current increases with increasing the scan rate, while the specific capacitance diminishes because of the less time of contact between electrode active sites and electrolyte interface. Table 4.3 provides the variations of specific capacitance with scan rates for the three-electrode and symmetric two-electrode systems.

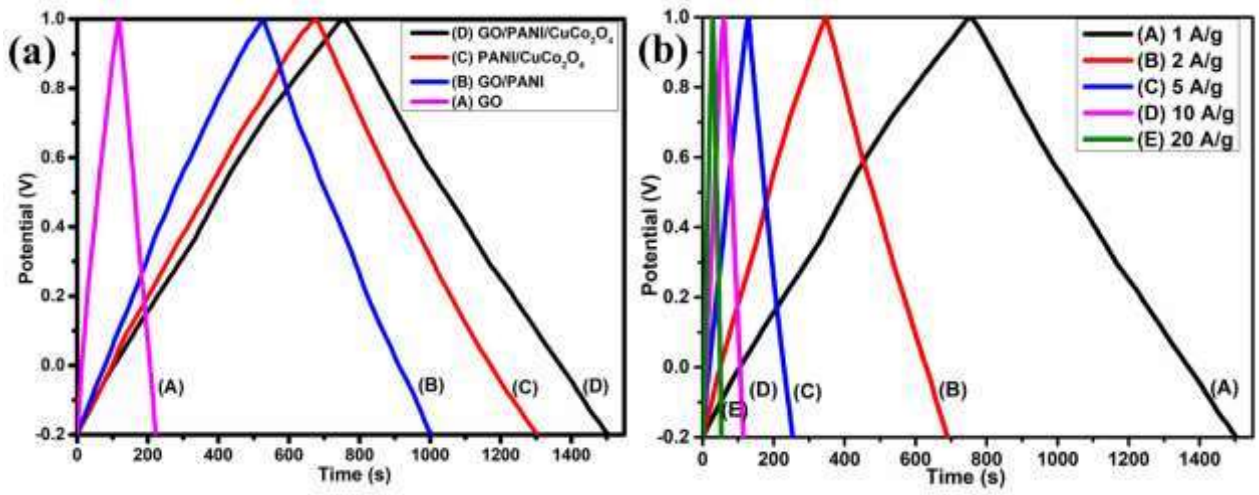

Figure 4.8: CD curve at (a) 1 A/g. (b) 1 A/g, 2 A/g, 5 A/g, 10 A/g, and 20 A/g of different samples

Moreover, the performance of the synthesized electrodes has also been examined from the symmetric two-electrode CD curve at a constant current density of 1 A/g (figure 4.8 (a)). It could be seen that GO/PANI/$CuCo_2O_4$ ternary composite has a high charge-discharge time compared to other prepared samples, and this high value of charge-discharge time is responsible for maximum specific capacitance value as specific capacitance is directly proportional to the discharge time (From the 2E CD equation). Figure 4.8 (b) shows the charge-discharge curve with various current density values from 1 A/g to 20 A/g for ternary composite GO/PANI/$CuCo_2O_4$ and it can be seen that charging-discharging time decreases with increasing the current density. For ternary composite GO/PANI/$CuCo_2O_4$, the lowest value of specific capacitance is observed at 20 A/g current density while the highest at 1 A/g. All the calculated value of specific capacitance from CD data have been shown in table 4.3. The inaccessible active sites of electrodes act as a barrier between the ion diffusion at high current density which result in lower value of specific capacitance.

Table 4.3: Specific capacitance values for three-electrode and symmetric two-electrode system

Material	**Scan rate (mV/s)**	**CV 3E C_s (F/g)**	**CV 2E C_s (F/g)**	**Current density (A/g)**	**CD 2E C_s (F/g)**
GO	1	153.41	45.79	1	43.89
GO/PANI	1	588.42	214.61	1	199.64
PANI/$CuCo_2O_4$	1	714.64	255.47	1	260.52

GO/PANI/$CuCo_2O_4$	1	741.39	308.15	1	312.72
GO/PANI/$CuCo_2O_4$	2	679.48	261.12	2	286.07
GO/PANI/$CuCo_2O_4$	5	602.08	214.52	5	261.44
GO/PANI/$CuCo_2O_4$	10	518.93	179.36	10	233.67
GO/PANI/$CuCo_2O_4$	20	445.16	153.44	20	208.83

The effect of specific capacitance with different values of scan rate in both two-electrode and three-electrode systems has been shown in figure 4.9 (a). It suggests that specific capacitance in symmetric two-electrode and three-electrode decreases as the scan rate is increased. The charge deliverability and storage capacity of the supercapacitor is described by specific power and specific energy; the values are found from equations 4.8 and 4.9, respectively,

$$P_{sp} = \frac{Esp}{td} \tag{4.8}$$

$$E_{sp} = \frac{1}{2} C_s V^2 \tag{4.9}$$

E_{sp} = specific energy of two-electrode configuration (Wh/kg); P_{sp} = specific power of two-electrode configuration (W/kg); C_s = specific capacitance of two-electrode configuration (F/g); V = stable potential window (Volt); t_d = discharge time of electrode (s)

Figure 4.9 (b) exhibits the Ragone plot (between specific energy and specific power) of the fabricated system. GO/PANI/$CuCo_2O_4$ ternary composite has a highest specific energy than binary PANI/$CuCo_2O_4$, GO/PANI, and pristine GO. Table 4.4 summarize the specific energy

and specific power values of different electrode material for symmetric two-electrode system. In table 4.4, it can be seen that the specific power values of all fabricated electrodes are almost equal, but the specific energy of the ternary GO/PANI/$CuCo_2O_4$ composite is the highest. This confirms that although all the devices have the same ability to deliver the stored charge, the ternary system has the maximum charge storage capacity. Hence, the performance of ternary composite was evaluated at different current densities. It was found that the specific energy values were continuously decreasing, while specific power was increasing with increase in current density. For ternary composite GO/PANI/$CuCo_2O_4$, the maximum specific energy was 62.545 Wh/kg with 300.042 W/kg specific power at 1 A/g current density. As current density was increased up to 20 A/g, specific energy reduced to 41.767 Wh/kg, and optimum specific power was obtained as 5997.613 W/kg. This high value of specific energy and specific power states that ternary composite GO/PANI/$CuCo_2O_4$ is highly reliable and more electrochemically active than other systems.

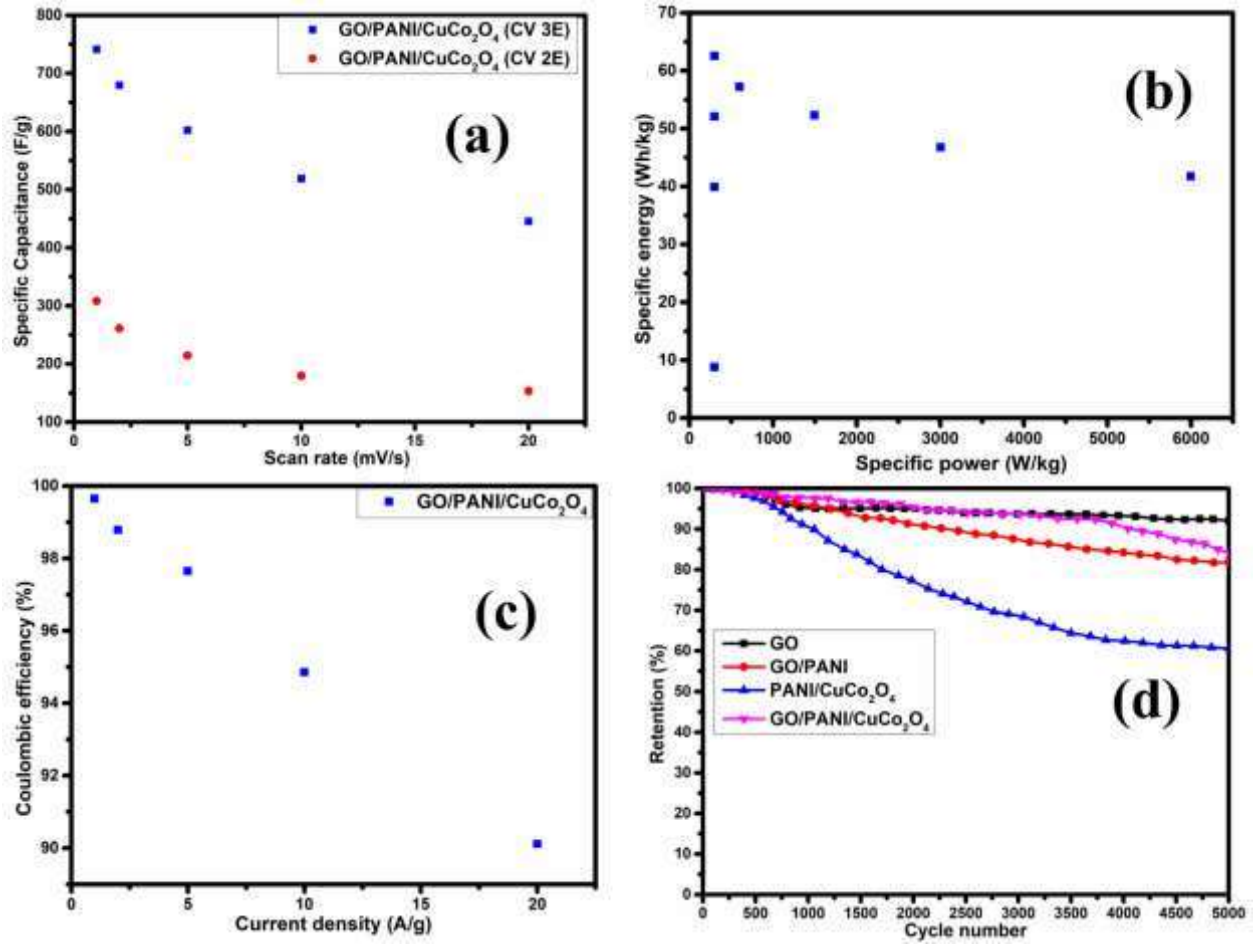

Figure 4.9: (a) Variation of specific capacitance with scan rate for three-electrode and symmetric two-electrode system. (b) Ragone plot (specific energy vs specific power of symmetric system). (c) Coulombic efficiency variation with different values of current density for ternary material. (d) Specific capacitance retention (%) plot after 5000 cycles

Coulombic efficiency is the charge transfer ability of the system. It is calculated from the charge-discharge plot of the symmetric systems by using equation 4.10.

$$\eta\,(\%) = \frac{td}{tc} * 100 \qquad (4.10)$$

η (%) = Two-electrode coulombic efficiency (%); t_d = discharge time (s); t_c = charge time (s)

Figure 4.9 (c) shows the relation between coulombic efficiency (%) and different value of current density (A/g). It is seen that coulombic efficiency decreases with an increase in current density. This could be due to the irreversible nature during charging-discharging or higher polarization zone. Ternary GO/PANI/$CuCo_2O_4$ exhibits a relatively good coulombic efficiency of 90.11 % even at a higher current density of 20 A/g.

Table 4.4: Specific energy and specific power values from symmetric two-electrode system

Material	Current density (A/g)	Specific energy (Wh/kg)	Specific power (W/kg)
GO	1	8.778	300.010
GO/PANI	1	39.928	300.029
PANI/$CuCo_2O_4$	1	52.104	300.025
GO/PANI/$CuCo_2O_4$	1	62.545	300.042
GO/PANI/$CuCo_2O_4$	2	57.215	598.921
GO/PANI/$CuCo_2O_4$	5	52.289	1497.112
GO/PANI/$CuCo_2O_4$	10	46.735	3006.501
GO/PANI/$CuCo_2O_4$	20	41.767	5997.613

Figure 4.9 (d) shows the percentage of retention for different cycle number. 5000 CV cycles were done to check the cycling stability of the fabricated electrode materials at a scan rate

of 100 mV/s. Ternary GO/PANI/$CuCo_2O_4$ composite has the highest capacitance retention of 84.25 % which is higher than binary PANI/$CuCo_2O_4$ and GO/PANI after the completion of 5000 cycles. GO also has excellent cycle stability of 92.04 % but does not have large specific capacitance because of the unavailability of redox (oxidation-reduction) reactions. It is well known that PANI and $CuCo_2O_4$ based electrode materials have poor cycle stability because of irregular volume expansion and some shrinkage during the charge-discharge cycles. When GO was added in PANI/$CuCo_2O_4$ binary composite, a better cycle stability was obtained for ternary composite GO/PANI/$CuCo_2O_4$. GO must be acting as a support to the backbone of PANI and $CuCo_2O_4$, thereby restricting the structural damages.

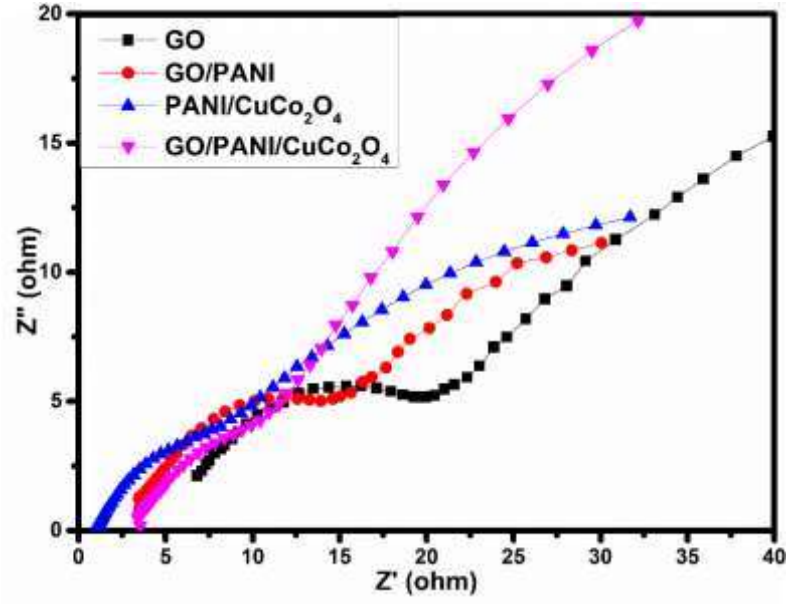

Figure 4.10: Nyquist plot of different samples

Furthermore, EIS was done in 1M KOH electrolyte to find out the various types of resistance like equivalent series resistance (R_s), charge transfer resistance (R_{ct}), Warburg impedance (w), EDLC, and pseudocapacitive behavior of the supercapacitors. The Nyquist plot has been shown in figure 4.10. R_s can be found by the x-axis intercept of the plotted quasi-semicircle.

The diameter of the formed semicircle is R_{ct} value. R_s is the combination of electrolyte solution resistance, material resistance, and resistance due to the contact between active material and electrolyte solution. The low-frequency region in the Nyquist plot displays the higher straight line for GO/PANI/$CuCo_2O_4$ compared to the other prepared samples, which suggests its better supercapacitive nature. The higher vertical slope resembled fast electrode kinetics and exhibited high power density. The large ion diffusion is assigned to the better electrode-electrolyte contact and more active sites of GO/PANI/$CuCo_2O_4$ which must be favoring the deep ion penetration between layers of GO/PANI/$CuCo_2O_4$. The equivalent series resistance and charge transfer resistance has been shown in table 4.5.

Table 4.5: R_s and R_{ct} values of samples

Material	R_s (Ω)	R_{ct} (Ω)
GO	5.66	19.76
GO/PANI	2.95	16.20
PANI/$CuCo_2O_4$	1.14	15.61
GO/PANI/$CuCo_2O_4$	3.25	12.23

Similarly, R_{ct} values of GO, GO/PANI, PANI/$CuCo_2O_4$, and GO/PANI/$CuCo_2O_4$ are found as 19.76 Ω, 16.20 Ω, 15.61 Ω, and 12.23 Ω. The decreased values of R_{ct} indicate improved electronic conductivity of the samples. GO/PANI/$CuCo_2O_4$ has the lowest R_{ct} value of 12.23 Ω, which must be due to the large number of active sites existence in the sample and the smooth flow of electrolyte ions.

The equivalent circuit diagrams corresponding to the different prepared systems have been shown in figure 4.11. The different equivalent circuits for all prepared samples could be due to the different internal mechanisms of ion transportation during charging-discharging. There are mainly seven types of resistance present in all synthesized samples including capacitance due to the two types of capacitance such as EDLCs and pseudocapacitance, constant phase element (Q) which shows the non-ideality of the supercapacitor due to the interface film resistance and some electrolyte barriers.

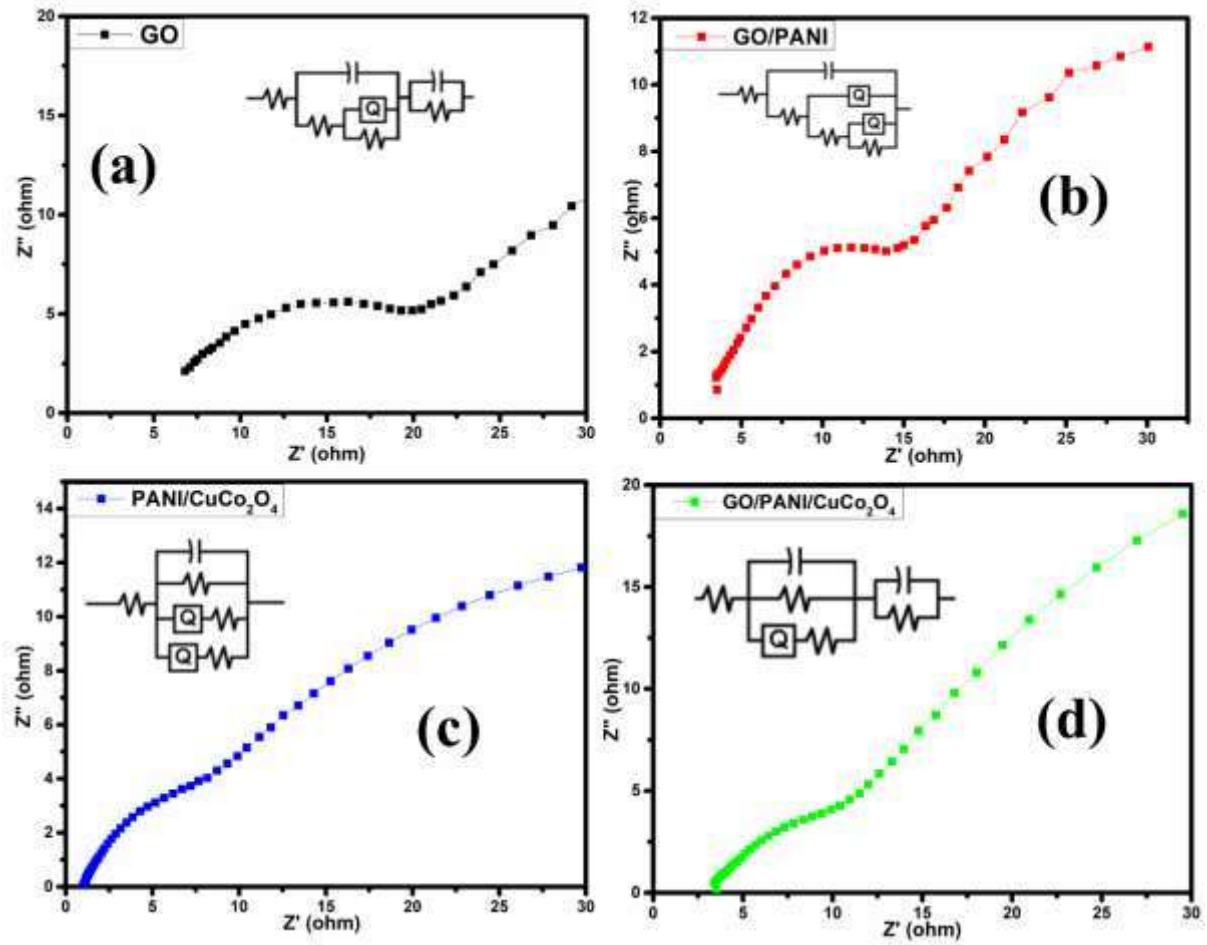

Figure 4.11: Equivalent circuit diagram from Nyquist data

Figure 4.12 (a) shows the variation of admittance values between the real and imaginary axis from where response time of the prepared samples can be found. Response time (t_r) is the time that suggests how fast a system can respond after providing proper input. It is inversely proportional to the knee frequency (f_k) according to equation 4.11.

$$t_r = \frac{1}{fk} \tag{4.11}$$

f_k is the frequency at which all the stored charges of the system can be utilized properly. The values of the f_k and t_r of different samples are shown in table 4.6. The t_r for GO is very low due to its EDLC nature, in which only physical adsorption can happen. But the response time for ternary composite GO/PANI/$CuCo_2O_4$ is very high, this is mainly because of the large number of redox reactions happening onto the electrode surface, which takes too much time for the competition compared to other synthesized materials.

Table 4.6: f_k and t_r values of samples

Material	f_k (Hz)	t_r (ms)
GO	125.89	7.94
GO/PANI	79.43	12.58
PANI/$CuCo_2O_4$	50.11	19.95
GO/PANI/$CuCo_2O_4$	1.58	632.91

Figure 4.12 (b) shows the |Z| vs frequency plot of supercapacitors with GO, GO/PANI, PANI/$CuCo_2O_4$, and GO/PANI/$CuCo_2O_4$ respectively. It can be stated that total impedance

|Z| is more at low frequency and less at high frequency. As the frequency is increased, the value of total impedance |Z| decreases. At low frequency, the total impedance |Z| of GO/PANI/$CuCo_2O_4$ is the least and for GO, its value is highest. This proves that the resistance in GO/PANI/$CuCo_2O_4$ is the lowest whereas it is quite high for GO. It was already being confirmed from the results of the Nyquist plot, where the R_{ct} value of GO/PANI/$CuCo_2O_4$ was the lowest. Figure 4.12 (c) displays the plot between admittance |Y| and frequency. As the frequency is increased, the value of the admittance |Y| also increases. Admittance |Y| is the reciprocal of impedance. The value of admittance |Y| is the highest for GO/PANI/$CuCo_2O_4$ at low frequency as compared to other samples, which could be due to its more conducting nature. But at the high frequency, the ions move faster, thus creating higher admittance values for all the synthesized materials.

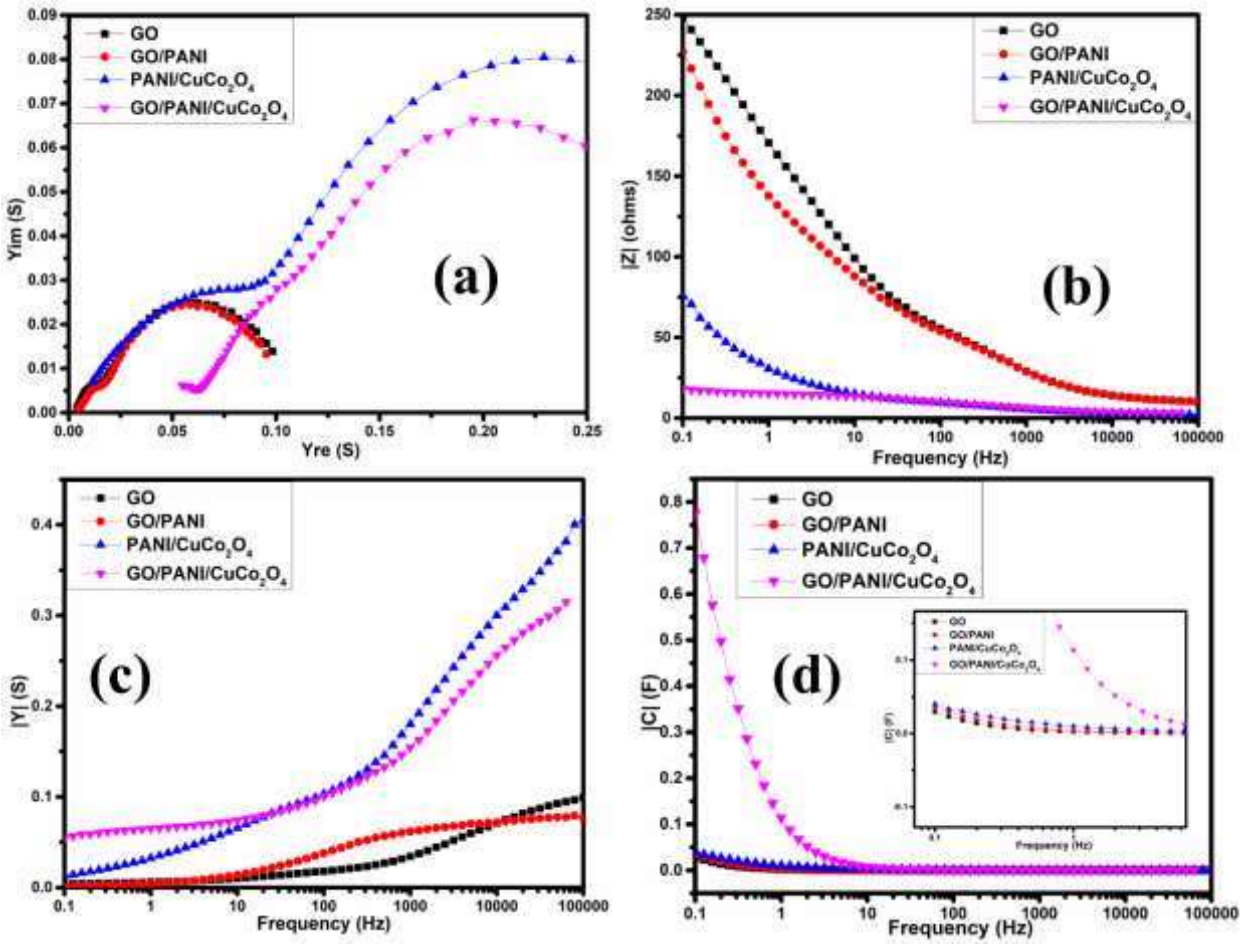

Figure 4.12: (a) Admittance variation in real and imaginary axis. (b) Total impedance (|Z|) vs frequency. (c) Total admittance (|Y|) vs frequency. (d) Total capacitance (|C|) vs frequency

The variation of capacitance and frequency is given in figure 4.12 (d). At low frequency, ternary GO/PANI/$CuCo_2O_4$ had the highest capacitance among all the synthesized samples. GO/PANI/$CuCo_2O_4$ sustained a better capacitance value for a broader range of frequencies than GO, GO/PANI, and PANI/$CuCo_2O_4$ at higher frequencies. It can be seen that at high frequency, the capacitance value was constant for all prepared samples. At low frequency, more electrolyte ions are available at the electrode-electrolyte interface, which resulted in increased values of capacitance.

For the ternary GO/PANI/$CuCo_2O_4$ system, a high value of specific capacitance was obtained than other prepared systems. The presence of GO in GO/PANI/$CuCo_2O_4$ ternary mostly restrain the volumetric contraction and expansion of PANI. Less contraction expansion of PANI molecules resulting high cycle stability of ternary than binary composite. Furthermore, the entrance of $CuCo_2O_4$ particles in the ternary system improves the charge transport mechanism. Hence, the synergistic effect of all the components in the composite developed a powerful electrode material.

4.3. Conclusion

In summary, ternary composite GO/PANI/$CuCo_2O_4$ showed superior electrochemical behavior for a supercapacitor active electrode material than other synthesized binary and a single material. The ternary GO/PANI/$CuCo_2O_4$ showed a high specific capacitance of 741.39 F/g and 312.72 F/g at 1 mV/s scan rate and 1 A/g current density using a three-electrode system and symmetric two-electrode system, respectively. The ternary GO/PANI/$CuCo_2O_4$ also exhibited high specific energy of 62.54 Wh/kg, 5997.61 W/kg specific power, and 84.25 % cyclic stability up to 5000 cycles. Hence, ternary GO/PANI/$CuCo_2O_4$ can be considered as a good candidate for supercapacitor electrode material with high specific energy and longer cyclic stability.